Turkish J. Eng. Env. Sci.
30 (2006) , 331 – 350.

A Simulation Model for a Single Cylinder Four-Stroke Spark Ignition Engine Fueled with Alternative Fuels

Maher A. R. Sadiq AL-BAGHDADI
Mechanical and Energy Department, Higher Institute of Mechanical Engineering, Yefren-LIBYA
e-mail: maherars@hotmail.com

Received 11.10.2004

Abstract

Considering the energy crises and pollution problems today, investigations have concentrated on decreasing fuel consumption by using renewable alternative fuels and on lowering the concentration of toxic components in combustion products. A simulative model for establishing the performance parameters of spark ignition engines fueled with a range of fuels (gasoline, ethanol, or hydrogen) and their mixture is presented. The incidence of pre-ignition and its relative intensity as well as cyclic variations are also accounted for. The 2-zone incorporates a procedure for deriving an estimate of the effective duration of combustion and the associated mass burning rate for various operating conditions and fuels. A system of first-order ordinary differential equations was obtained for the pressure, mass, volume, temperature of the burned and unburned gases, heat transfer from the burned and unburned zone, mass flow into and out of crevices, and the composition of combustion products. The mathematical and simulation model has been developed, tested, and verified against the experimental data to simulate a 4-stroke cycle of a spark ignition engine fueled with gasoline, ethanol, or hydrogen as a single fuel or their mixture. The results obtained from the present study have shown the capability of the model to predict satisfactorily the performance and emissions including the incidence of pre-ignition at various engine-operating conditions. A good agreement was obtained between the results of the present model and the experimental results.

Key words: Power generation, Pollution, ICE, Spark ignition engine model, Simulation model, Thermodynamics, Hydrogen, Ethanol, Alternative fuel.

Introduction

Considering the energy crises and pollution problems today, investigations have concentrated on decreasing fuel consumption by using alternative fuels and on lowering the concentration of toxic components in combustion products. Hydrogen is considered an ideal alternative fuel. The use of hydrogen as an automotive fuel, as a primary or supplementary fuel, appears to promise a significant improvement in the performance of a spark ignition engine. Besides being the cleanest burning chemical fuel, hydrogen can be produced from water (using non-fossil energy) and, conversely, on combustion forms water again by closed cycle (Veziroglu et al. 1989; Veziroglu and Barbir, 1991, 1992). A small amount of hydrogen mixed with gasoline and air produces a combustible mixture, which can be burned in a conventional spark ignition engine at an equivalence ratio below the lean flammability limit of a gasoline/air mixture. The resulting ultra-lean combustion produces a low flame temperature and leads directly to lower heat transfer to the walls, higher engine efficiency and lower exhaust of CO and NOx (Sher and Hacohen, 1987; Al-Baghdadi, 2000, 2002).

Ethanol is a likely alternative automotive fuel in that it has properties that would allow its use in present engines with minor modifications. Alcohol fuels can be made from renewable resources like locally grown crops and even waste products such as

waste paper or grass and tree trimmings (Morris, 1992). As a fuel for spark-ignition engines, ethanol has some advantages over gasoline, such as better anti-knock characteristics and reduction of CO and UHC emissions. Ethanol fuel has a high heat of vaporization; therefore, it reduces the peak temperature inside the cylinder and hence reduces the NOx emissions and increases the engine power (Wei-Dong et al., 2002; Al-Hasan, 2003; Bang-Quan et al., 2003).

One of the major areas of development in the internal combustion engine is the development of computer simulations of various types of engines. Their economic value is in the reduction in time and costs for the development of new engines and their technical value is in the identification of areas that require specific attention as the design study evolves. Computer simulations of internal combustion engine cycles are desirable because of the aid they provide in design studies, in predicting trends, in serving as diagnostic tools, in giving more data than are normally obtainable from experiments, and in helping one to understand the complex processes that occur in the combustion chamber. In the present work, a quasi-dimensional model was developed to simulate a 4-stroke cycle of a spark ignition engine fueled with various types of fuels, i.e. gasoline, hydrogen, ethanol, and their mixture.

Modeling of The Spark Ignition Engine (Power Cycle)

The combustion chamber was generally divided into burned and unburned zones separated by a flame front (Figure 1). The first law of thermodynamics, equation of state and conservation of mass and volume were applied to the burned and unburned zones. The pressure was assumed to be uniform throughout the cylinder charge. A system of first-order ordinary differential equations was obtained for the pressure, mass, volume, temperature of the burned and unburned zones, heat transfer from burned and unburned zone, and mass flow into and out of crevices.

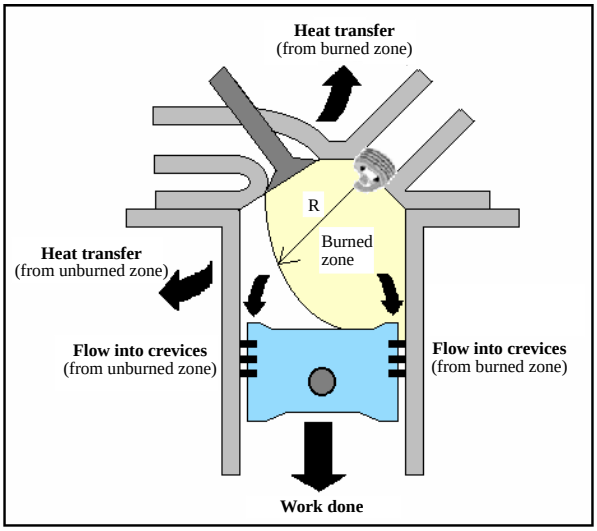

Figure 1. Two-zone thermodynamic model of combustion.

The mass burning rate was modeled by the following equation (Heywood, 1989):

$$\frac{dM_b}{dt} = A_{fl}.\rho.ST \tag{1}$$

The turbulent flame front speed (ST) was modeled by the following equation (Heywood, 1989):

$$ST = SL.f.\frac{(\rho_u/\rho_b)}{[(\rho_u/\rho_b)-1]\,Xm_b+1} \tag{2}$$

where f is a turbulent flame factor, defined with the following formula:

$$f = 1 + 0.0018 \times rpm \tag{3}$$

The laminar flame front speed for mixtures of hydrocarbon and/or alcohol with hydrogen, air, and residual gas was modeled by the following equation (Yu et al., 1986):

$$SL = SL_o.\left(\frac{T_u}{T_o}\right)^{\alpha}.\left(\frac{P}{P_o}\right)^{\beta}.\left(1-2.06Xr^{0.77}\right) + 0.83 \times YH_2 \tag{4}$$

where YH_2 is an indication of the relative amount of hydrogen addition, which was defined by the following formula:

$$YH_2 = \left(\frac{[H] + \frac{[H]}{([H]/[Air])_{st}}}{[F] + \left([Air] - \frac{[H]}{([H]/[Air])_{st}} \right)} \right) \quad (5)$$

For pure hydrocarbon fuels or pure alcohol fuel, $YH_2 = 0$

$$\alpha = 2.18 - 0.8\,(\phi - 1) \quad (6)$$

$$\beta = -0.16 + 0.22\,(\phi - 1) \quad (7)$$

$$SL_o = B2 + B3\,(\phi - B1) \quad (8)$$

Values of B1, B2 and B3 are given by Heywood (1989) for several types of fuels.

For a pure hydrogen fuel, the following semi-empirical formula suggested by Fagelson et al. (1978) was used for turbulent flame front speed:

$$\begin{aligned} ST_{H_2} &= 5000\left(0.1 rpm.B.S.P/T_b^{1.67}\right)^{0.4}. \\ &\left(T_b^{0.41}.T_u^{1.25}\right).\left(\frac{R}{E}\right) \\ &\times \left(\frac{Xf.\left(1 - \phi.\left(1 - \frac{R.T_b^2}{E.(T_b - T_u)}\right)\right)}{\phi} \right)^{0.5} \\ &\times \exp\left(\frac{-E}{2.R.T_b}\right) \end{aligned} \quad (9)$$

The liquid fuel (gasoline and ethanol) enters the air stream through the liquid fuel discharge tube in the carburetor body and is atomized and convected by the air stream past the throttle plate and into the intake manifold (Figure 2). Liquid fuel evaporation starts within the carburetor and continues as fuel droplets move with the air stream. Gas fuel (hydrogen) is mixed with the liquid fuel-air mixture before the throttle valve to enter the intake manifold.

For single fuel, the following formula was used to calculate the equivalence ratio:

$$\phi = \frac{\left(\frac{[F]}{Air}\right)_{Act.}}{\left(\frac{[F]}{[Air]}\right)_{st.}} \quad (10)$$

For the blending of hydrocarbon and/or alcohol with hydrogen fuel, the equivalence ratio was calculated from the following formula:

$$\phi = \frac{\left(\frac{[F]}{[Air] - \frac{[H]}{([H]/Air)_{st.}}}\right)}{\left(\frac{[F]}{[Air]}\right)_{st.}} \quad (11)$$

The flame front area (A_{fl}) calculations were based on the model of Annand (1970).

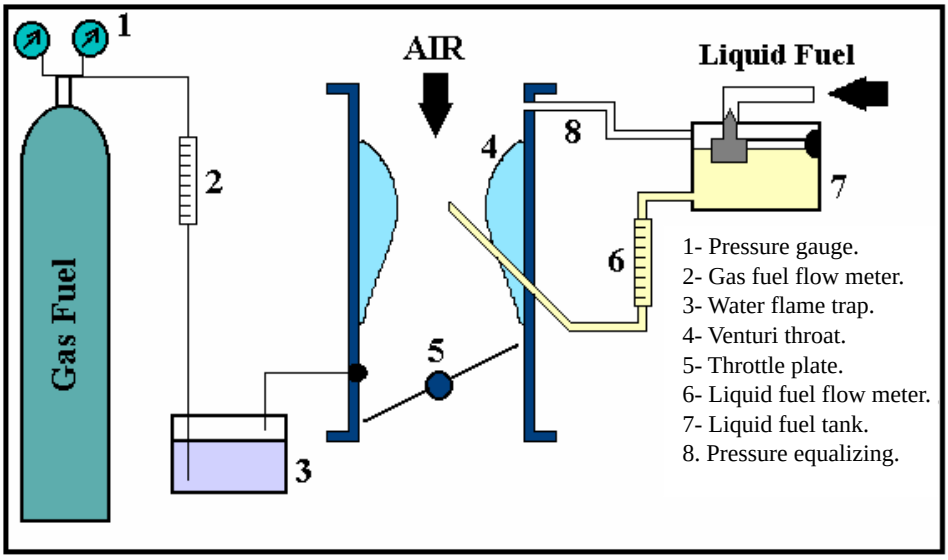

Figure 2. Schematic of fuel supply to the engine.

The instantaneous heat interaction between the cylinder content (burned and unburned zones) and its walls was calculated by using the following semi-empirical expression for a 4-stroke engine (Al-Baghdadi and Al-Janabi, 1999):

$$-\frac{dQ_{ht}}{dt} = A\left[0.26\frac{k}{B}\left(\frac{Up.B}{\mu}\right)^{0.7}(T-T_w) + 0.69\sigma\left(T^4-T_w^4\right)\right] \quad (12)$$

The crevices are the volumes between the piston, piston rings and cylinder wall (Figure 1). Gases flow into and out of these volumes during the engine operating cycle as the cylinder pressure changes. The instantaneous energy flows into the crevices were calculated by using the following semi-empirical expression of Gatowski et al. (1985) for a spark ignition engine:

$$\frac{dQ_{cr}}{d\theta} = (e+R.T).\frac{dN_{cr}}{d\theta} \quad (13)$$

where $dN_{cr} > 0$ when flow is out of the cylinder into the crevice, $dN_{cr} < 0$ when flow is from the crevice to the cylinder, and (e+R.T) is evaluated at cylinder conditions when $dN_{cr} > 0$ and at crevice conditions when $dN_{cr} < 0$.

In a conventional spark ignition engine the fuel and air are mixed together in the intake system, inducted through the intake valve into the cylinder, where mixing with residual gas takes place, and then compressed. Under normal operating conditions, combustion is initiated towards the end of the compression stroke at the spark plug by an electric discharge. Following inflammation, a turbulent flame develops, propagates through this essentially premixed fuel, air, burned gas mixture until it reaches the combustion chamber walls, and then extinguishes to begin the expansion stroke until the exhaust valve opening. Each of these processes is discussed below to complete an engine power cycle simulation.

The compression process starts at the trapped condition, and ends after the delay period process, when the mixture is ignited by the spark plug. Using a perfect mixing model for fresh charge and residuals from the previous cycle derives the state of the gas during this stage.

The gas pressure and temperature during the compression stage are calculated using the following equations:

$$\frac{dP}{d\theta} = \left[-\left(1+\frac{R}{C_v}\right).P.\frac{dV}{d\theta} - \frac{R}{C_v}.\frac{dQ_{cr}}{d\theta} + \frac{R}{C_v}.\frac{dQ_{ht}}{d\theta}\right]\Big/V \quad (14)$$

$$\frac{dT}{d\theta} = T.\left(\frac{1}{P}.\frac{dP}{d\theta} + \frac{1}{V}.\frac{dV}{d\theta}\right) \quad (15)$$

The numerical method used for this purpose is the Runge-Kutta method.

After spark occurrence, the delay period is calculated using the following equation:

$$DP = \left[\left(\frac{6.rpm}{ST}\right).\sqrt[3]{\left(\frac{0.001V}{\pi}\right)}\right] \quad (16)$$

During this period, the mixture is considered unburned and the compression process is continued. The process continues for as many time intervals as necessary until the total angle from the nominal spark timing is greater than the delay period. The combustion process is said to have commenced, and is divided into 2 stages. The first stage is ignition and initiation of 2 zones in combustion space and the second stage is flame front propagation.

After the combustion of the small nucleus of the fuel-air mixture the combustion chamber is subdivided into 2 zones, a burned zone, suffix (b), and an unburned zone, suffix (u). The process is initiated in 3 steps based on the model of Benson et al. (1975).

The cylinder pressure and the temperature of burned and unburned zones of the flame front propagation stage were modeled using the following equations:

$$\frac{dT_u}{d\theta} = \frac{1}{N_u.C_{p,u}}.\frac{dQ_{ht,u}}{d\theta} + \frac{V_u}{N_u.C_{p,u}}.\frac{dP}{d\theta} - \frac{1}{N_u.C_{p,u}}.\frac{dQ_{cr,u}}{d\theta} \quad (17)$$

$$\frac{dT_b}{d\theta} == \frac{P}{N_b.R}.\left[\frac{dV}{d\theta} - \left(\frac{R.T_b}{P} - \frac{R.T_u}{P}.\frac{MW_b}{MW_u}\right).\frac{dN_b}{d\theta} - \frac{V_u.R}{P.C_{p,u}}.\frac{dP}{d\theta} - \frac{R}{P.C_{p,u}}.\frac{dQ_{ht,u}}{d\theta} + \frac{R}{P.C_{p,u}}.\frac{dQ_{cr,u}}{d\theta} + \frac{V}{P}.\frac{dP}{d\theta}\right] \tag{18}$$

$$\frac{dP}{d\theta} = \left[\frac{\left[p\frac{dV}{d\theta}.\left(1+\frac{C_{v,b}}{R}\right) + \left(\frac{C_{v,u}}{C_{p,u}} - \frac{C_{v,b}}{C_{p,u}}\right).\frac{dQ_{ht,u}}{d\theta} + \left(e_b - e_u.\frac{MW_b}{MW_u}\right).\frac{dN_b}{d\theta}\right]}{\left[\frac{C_{v,u}}{C_{p,u}}.V_u - \frac{C_{v,b}}{C_{p,u}}.V_u + \frac{C_{v,b}}{R}.V\right]} - \frac{\left(C_{v,b}.\left(T_b - T_u.\frac{MW_b}{MW_u}\right)\right).\frac{dN_b}{d\theta} + \left(\frac{C_{v,b}}{C_{p,u}} - \frac{C_{v,u}}{C_{p,u}}\right).\frac{dQ_{cr,u}}{d\theta} + \frac{dQ_{cr}}{d\theta} - \frac{dQ_{ht}}{d\theta}\right]}{\left[\frac{C_{v,u}}{C_{p,u}}.V_u - \frac{C_{v,b}}{C_{p,u}}.V_u + \frac{C_{v,b}}{R}.V\right]}\right] \tag{19}$$

Equations (17), (18) and (19) are solved by the Runge-Kutta method to calculate the unburned zone temperature, the burned zone temperature and the cylinder pressure, respectively, during each time step.

Once the combustion is complete the variables are organized to calculate for a single zone only. The Runge-Kutta method is used. Throughout the expansion calculation a check is kept to see if NO is frozen when the NO rate kinetic calculations are bypassed.

Twelve species were considered in the calculation of combustion product concentrations. The calculation starts from the equation of combustion of hydrocarbon, ethanol, hydrogen fuels and air, which is represented by

$$\begin{gathered} ae\left[(1-Z).(1-J)\,C_nH_m + Z(1-J)\,C_2H_5OH + JH_2\right] + \\ \frac{ae}{\phi}\left[n(1-Z)(1-J) + 3Z(1-J) + ((m.(1-Z)(1-J) + 2J)/4)\right]\left(O_2 + \frac{78}{21}N_2 + \frac{1}{21}Ar\right) \\ \longrightarrow X_{H_2O}H_2O + X_{H_2}H_2 + X_{OH}OH + X_HH + X_{N_2}N_2 + X_{NO}NO + X_NN \\ + X_{CO_2}CO_2 + X_{CO}CO + X_{O_2}O_2 + X_OO + X_{Ar}Ar \end{gathered} \tag{20}$$

The composition was calculated in terms of molar fractions of these species denoted by Xi. The equilibrium distribution of these species can be fully described by the following 7 reactions:

$$\frac{1}{2}H_2 \longleftrightarrow H \tag{21}$$

$$\frac{1}{2}O_2 \longleftrightarrow O \tag{22}$$

$$\frac{1}{2}N_2 \longleftrightarrow N \tag{23}$$

$$2H_2O \longleftrightarrow 2H_2 + O_2 \tag{24}$$

$$H_2O \longleftrightarrow OH + \frac{1}{2}H_2 \tag{25}$$

$$CO_2 + H_2 \longleftrightarrow H_2O + CO \tag{26}$$

$$H_2O + \frac{1}{2}N_2 \longleftrightarrow H_2 + NO \tag{27}$$

The calculations were based on the equilibrium assumption, except for NOx formation, where the extended Zeldovich mechanism was used.

$$\begin{gathered} N + NO \leftrightarrow N_2 + O \\ K1f = 3.1 \times 10^{10} \exp\left(\tfrac{-160}{T}\right) \end{gathered} \tag{28}$$

$$\begin{gathered} N + O_2 \leftrightarrow NO + O \\ K2f = 6.4 \times 10^{6}.T.\exp\left(\tfrac{-3125}{T}\right) \end{gathered} \tag{29}$$

$$N + OH \leftrightarrow NO + H$$
$$K3f = 4.2 \times 10^{10} \quad (30)$$

where K1f, K2f, and K3f are the forward rate constants, taken from the model of Benson et al. (1975).

Pre-ignition and knock in spark ignition engines are acknowledged barriers to the further improvement of efficiency, increased power and the use of a wider range of fuels. Pre-ignition is caused mainly by the auto-ignition of the fresh gas mixture of the charge before the spark ignition time during the compression stroke. This may lead to the incidence of peak cylinder pressure before top dead center and/or undesirable combustion. The onset of knock, which is caused mainly by the auto-ignition of the unburned mixture in the "end gas region" of the charge that is at any moment yet to be burned, involves exceedingly rapid rates of combustion of the fuel-air mixture, increased heat transfer to the cylinder walls, excessively high cylinder pressure and temperature levels, and increased emissions. The pre-ignition and knock lead to highly undesirable engine performance and potential damage to engine components when allowed to persist. Accordingly, it is critically important not only to avoid pre-ignition and knocking but also to know the limiting conditions for their incidence under any set of operating and designing conditions. The common approach to modeling the ignition delay is fitting an equation to the experimental data (Douaud and Eyzat, 1978). For different running conditions with pre-ignition and knock, the pressure and temperature of the fresh gas until pre-ignition or knock occurs are determined. The auto-ignition model can be formulated as follows:

$$\theta_{Auto-ignition} - \theta_{Start} = X_1 P(\theta)^{X_2} \exp\left(\frac{X_3}{T_u(\theta)}\right) \quad (31)$$

where $\theta_{Auto-ignition}$ is auto-ignition occurrence crank angle, θ_{Start} is the start of cycle, and X_1, X_2, and X_3 are experimental constants.

Optimization of the auto-ignition model with different engine operating conditions of fuel mixture, compression ratio, equivalence ratio, and spark timing showed that the model could be simplified by fixing the value of X1 at 0.757, the value of X2 at 0.896 and the value of X3 at 6471. Equation (31) was then used with a quasi-1-dimensional thermodynamic model (2-zone thermodynamic model) to predict the incidence of auto-ignition at various engine operating conditions. With this model, it is possible not only to investigate whether auto-ignition is observed with changing fuel mixture, operating and/or design parameters, but also to evaluate those parameters' effects on the maximum possible auto-ignition intensity.

The advantage of the hydrogen-supplemented fuel is that it requires a smaller quantity of hydrogen, which considerably reduces the problems connected with hydrogen storage in the automobile. The important improvements in ethanol addition are to reduce the NOx and CO emission while increasing the higher useful compression ratio and output power of a hydrogen-supplemented fuel engine. The least quantity of ethanol blended with gasoline and exactly satisfying constant NOx emission when hydrogen is added was calculated by using the semi-empirical expression of Al-Baghdadi, (2001) for safe operation of a spark ignition engine:

$$X_{ethanol} = 7 \times \ln(X_{hydrogen}) + 11 \quad (32)$$

The Computer Programme and Computational Procedure

The simulation of the power cycle of spark ignition engine was programmed using Visual Basic language (Figure 3). The computer program consists of a main part and 5 subroutines. During the power cycle, the program predicts the rate of mass burning, heat release rate, accumulated heat release, composition of burned and unburned zones, temperature of burned and unburned zones, cylinder pressure, heat loss by radiation and convection, energy loss due to flow into crevices, flame front speed, flame front radius, concentration of pollutants emitted, and engine performance. The flow chart of the main program is shown in Figure 4.

Experimental Work

Fuel properties of ethanol-gasoline blended fuels were examined by the standard ASTM methods. Unleaded gasoline, the base fuel, with research octane number equal to 95 (Table 1) was selected, and mixed with different percentages of ethanol (99.9% purity). From the results of the ASTM analysis, some of the combustion-related properties have been summarized in Table 1. The "E" designates ethanol and the number next to "E" designates the volume percentage of ethanol. The E10 means that 10% ethanol (99.9% purity) was blended with 90% pure gasoline by volume.

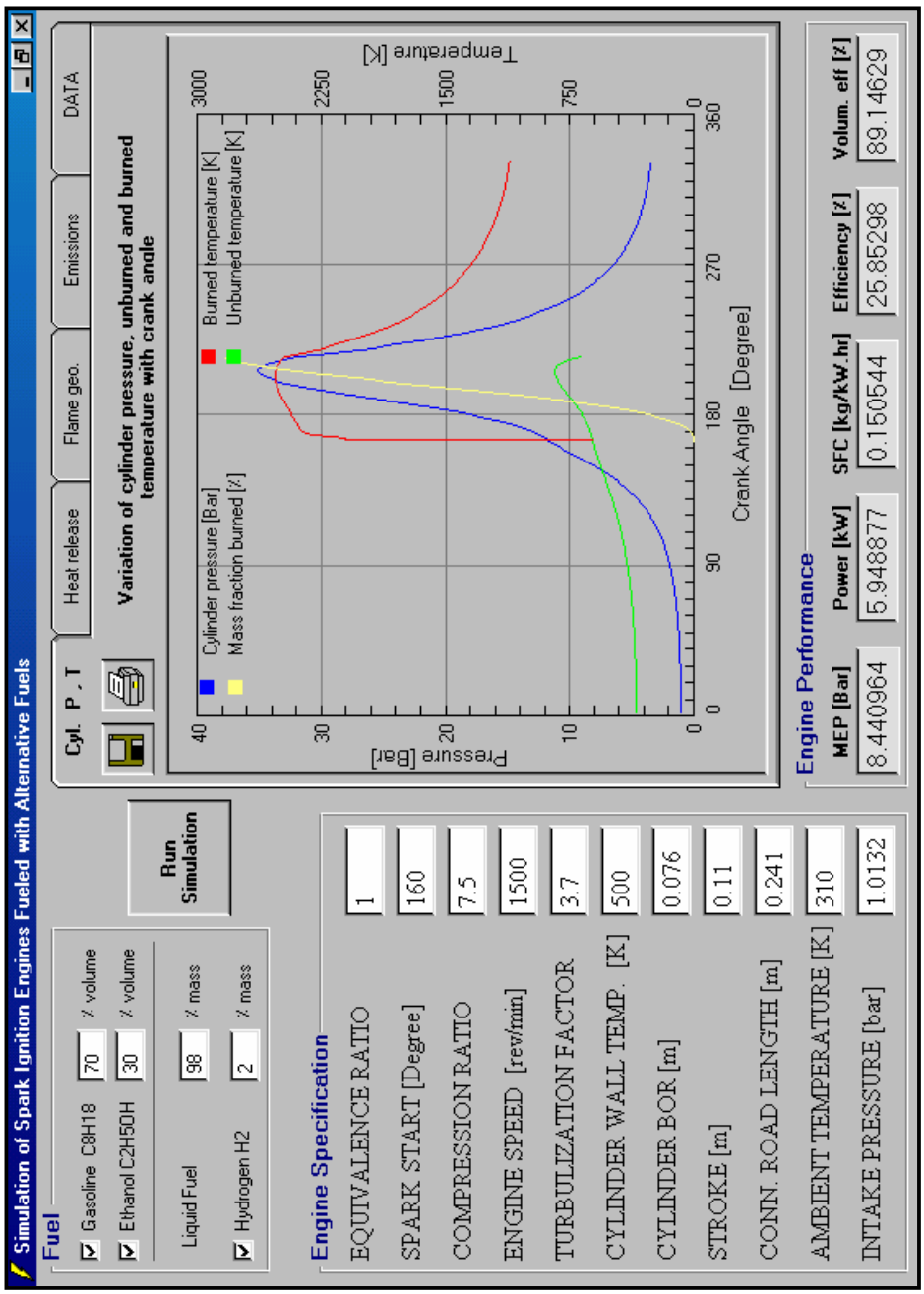

Figure 3. Visual interface of the SI simulation program.

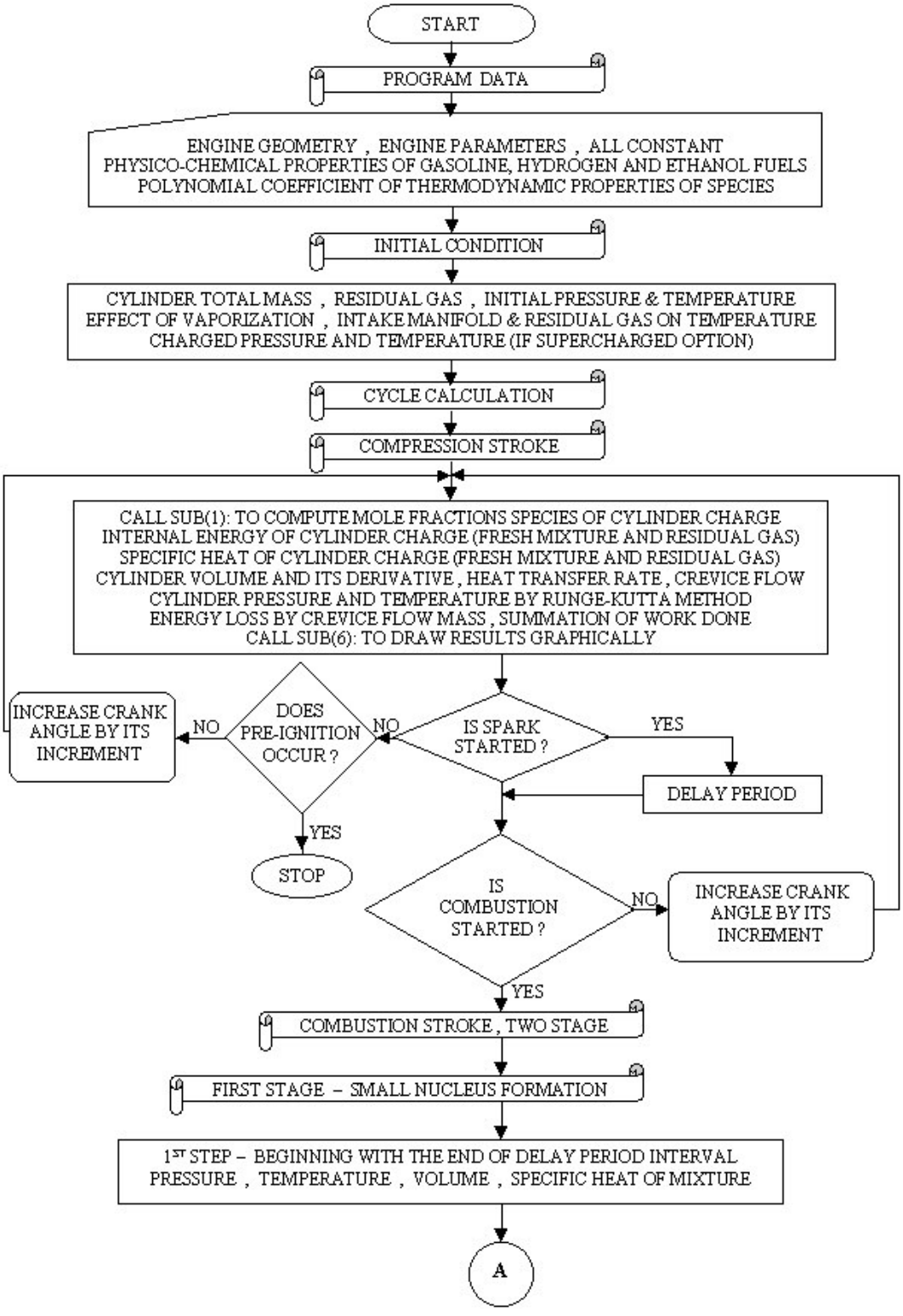

Figure 4a. Schematic flow chart of the cycle calculation computer program.

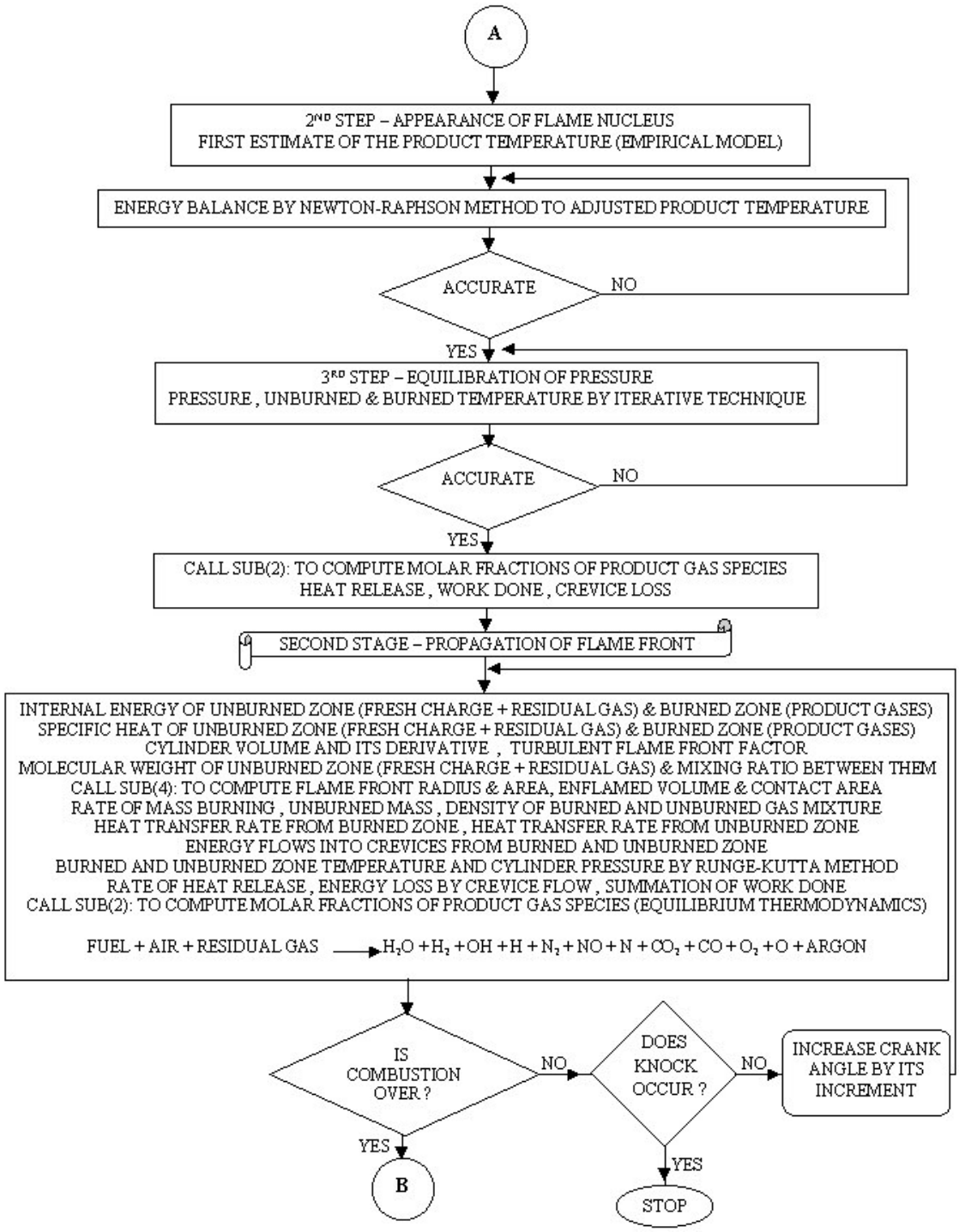

Figure 4b. Schematic flow chart of the cycle calculation computer program.

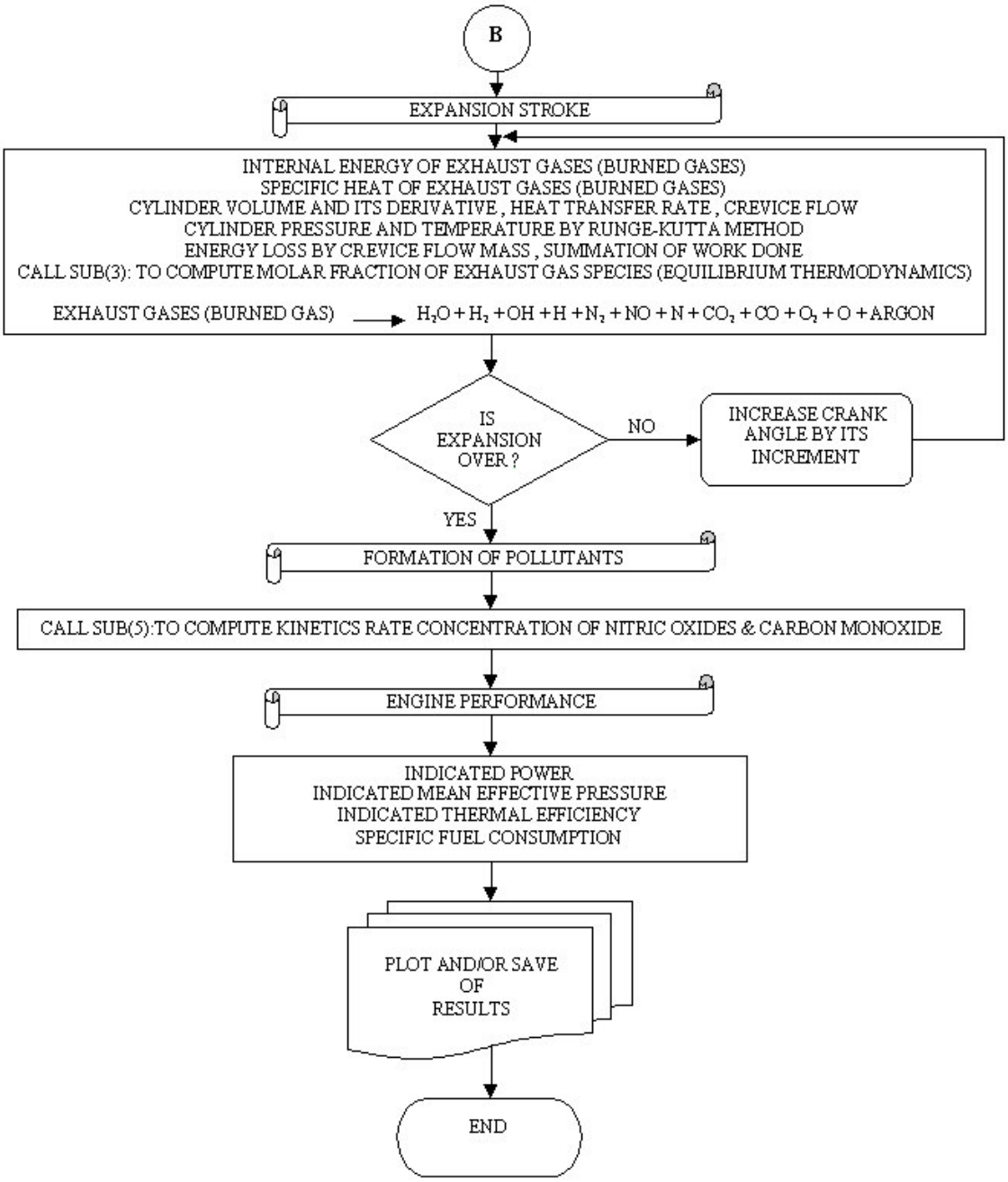

Figure 4c. Schematic flow chart of the cycle calculation computer program.

Table 1. Properties of different ethanol-gasoline blended fuels.

Property item	Gasoline	E10	E20	E30	Test method
Density (kg/l @ 15.5 °C)	0.772	0.775	0.777	0.780	ASTM D1298
RON	95	97.5	99.5	101	ASTM D2699
RVP (kPa @ 37.8 °C)	53.4	59.6	58.3	56.8	ASTM D323
Total Sulfur (wt%)	0.0074	0.0068	0.0059	0.0052	ASTM D4292
Existent Gum (mg/100 ml)	0.8	0.8	0.8	0.8	ASTM D381
Corrosivity (3 h @ 50 °C)	1a	1a	1a	1a	ASTM D130
Oxidation Stability Induction Period	> 360	> 360	> 360	> 360	ASTM D525
Distillation temperature (°C):					
IBP	35.5	37.8	36.7	39.5	ASTM
10 vol.%	54.5	50.8	52.8	54.8	D86
50 vol.%	94.4	71.1	70.3	72.4	
90 vol.%	167.3	166.4	163.0	159.3	
End point	197.0	197.5	198.6	198.3	
Heating value (kJ/kg)	42604.8	39820.6	39004.2	36341.4	
Carbon (wt.%)	86.6	86.7	87.6	86.0	
Hydrogen (wt.%)	13.3	13.2	12.3	13.9	
Residue (vol.%)	1.7	1.5	1.5	1.5	
Color	Light green				Visual

A Ricardo E6/US single cylinder research engine has been used in this research. The technical details of the engine are given in Table 2. The engine power has been measured using an electrical dynamometer. The exhaust gas was analyzed for CO by a non-dispersive infrared analyzer, NDIR, and for NOx by chemluminescent analyzer, CUSSONS equipment. A high-pressure transducer, type AVL-SQP, was used to record the cylinder head pressure. The transducer signal has been amplified by a CUSSONS-PIEZO channel amplifier, and then stored and presented on the display of a CRT Kikusui-COS5020-ST oscilloscope. A pick-up for an angle maker has been installed and its signal is also presented on the oscilloscope display. The incidence of auto-ignition was established directly from the observation of the cylinder pressure variation with time while using a flush-mounted pressure transducer.

Table 2. The technical details of the engine.

Type:	Ricardo E6/US, spark ignition engine
Cycle:	Four stroke
Number of Cylinder:	1
Cylinder Bore:	76.2 mm
Stroke:	110.0 mm
Connecting Rod Length:	241.3 mm
Compression Ratio:	variable
Engine Speed:	variable
Ignition Timing:	variable
Intake valve	
Diameter:	35 mm
Opens:	9° BTDC
Closes:	36° ABDC
Exhaust valve	
Diameter:	30 mm
Opens:	42° BTDC
Closes:	7° ABDC

Results

In hydrogen-fuelled spark ignition engine applications, the onset of pre-ignition or knock remains one of the prime limitations that needs to be studied so as to avoid its incidence and achieve superior performance. With the present model, it is possible not only to investigate whether pre-ignition or knock is observed with changing operating and design parameters, but also to evaluate their effects on the maximum possible auto-ignition intensity. In Figure 5, the average pre-ignition for 100 consecutive cycles is observed at 10° crank angle BTDC when the compression ratio is increased to 10.6. The pre-ignition occurrence crank angle prediction of the model at 10.7° crank angle timing is very accurate with a deviation of 0.7° crank angle. In Figure 6, the average pre-ignition for 100 consecutive cycles is observed at 6° crank angle BTDC when spark-timing is retarded 5° from the optimum spark timing (8° BTDC). The pre-ignition occurrence crank angle prediction of the model at 6.5° crank angle timing is very accurate; it is only a 0.5° crank angle deviation from the measured data.

As can be seen from Figures 5 and 6, the predicted pressure crank angle diagram coincides with the measured diagram; both the values and trends of the calculated pressures are in good agreement with the measured pressures. The error in maximum pressures is less than 4% for both cases and the deviation in pre-ignition occurrence crank angle is less than 1° crank angle.

Figures 7-9 show the measurements and predictions of the effect of hydrogen blending, (0%-12% by mass), and/or ethanol blending (0%-30% by volume), on the power and emission of the engine. The hydrogen-ethanol-gasoline fueled engine operates with a stoichiometric mixture, optimum spark timing for best torque, 1500 rpm and a 7.5 compression ratio. Each parameter studied is made dimensionless by relating it to its value when the engine is fueled with a pure gasoline at 7.5 compression ratio, 1500 rpm, stoichiometric mixture and optimum spark timing for best torque. The figures show that the results predicted by the mathematical model are very close (within 2%) to the experimental results. This verifies that the model developed can be used to a great degree of accuracy.

Figure 7 shows the effect of hydrogen and ethanol blending on the engine power. It is shown that engine power increases as the percentage of hydrogen blending is increased due to the high rate of mass burning of hydrogen. When the percentage of blending is more than 2%, the power decreases due to a reduction in mixture density and engine volumetric efficiency. The engine power increases with the increase in ethanol percentage volume ratio in the gasoline up to 30% ethanol; at this percentage the maximum brake power has been obtained due to the increase in mixture density and engine volumetric efficiency. During the tests, it is observed that the ethanol percentage exceeds 30%, the carburetor is not capable of evaporating all fuel supplied to the engine, and part of it enters the chamber without

combustion. This causes a reduction in the brake power and thermal efficiency as the ethanol percentage increases about 30%. Figure 8 shows the effect of hydrogen and ethanol blending on the specific fuel consumption (sfc). The sfc decreases as the percentage of hydrogen blending is increased until 6%. Then the decreases in sfc seem to be marginal throughout the percentage range. The sfc is slightly increased as the volume percentage of ethanol is increased in the mixture. This is due to the lower heating value of ethanol compared with gasoline. Figure 9 shows the effect of hydrogen and ethanol blending on CO emission. CO concentration decreases as the percentage of hydrogen and/or ethanol addition increases. This is due to the reduction in carbon atoms concentration in the blended fuel and the high molecular diffusivity of hydrogen, which improve the mixing process and hence combustion efficiency. Figure 10 shows the effect of hydrogen and ethanol blending on NOx emission. NOx concentration increases as the hydrogen mass ratio increases. This is due to the higher

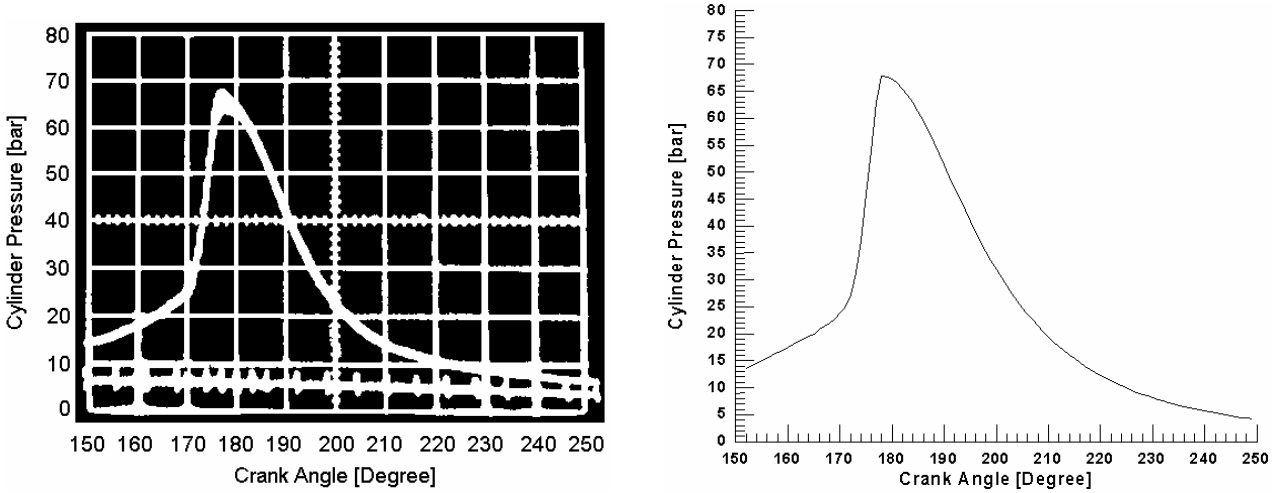

Figure 5. (a) Cylinder pressure with crank angles photograph and (b) model prediction indicating pre-ignition combustion (compression ratio = 10.6, equivalence ratio = 0.96, engine speed = 25 rev/s, Tin = 313 K, Pin = 1 bar, spark timing = 8° BTDC).

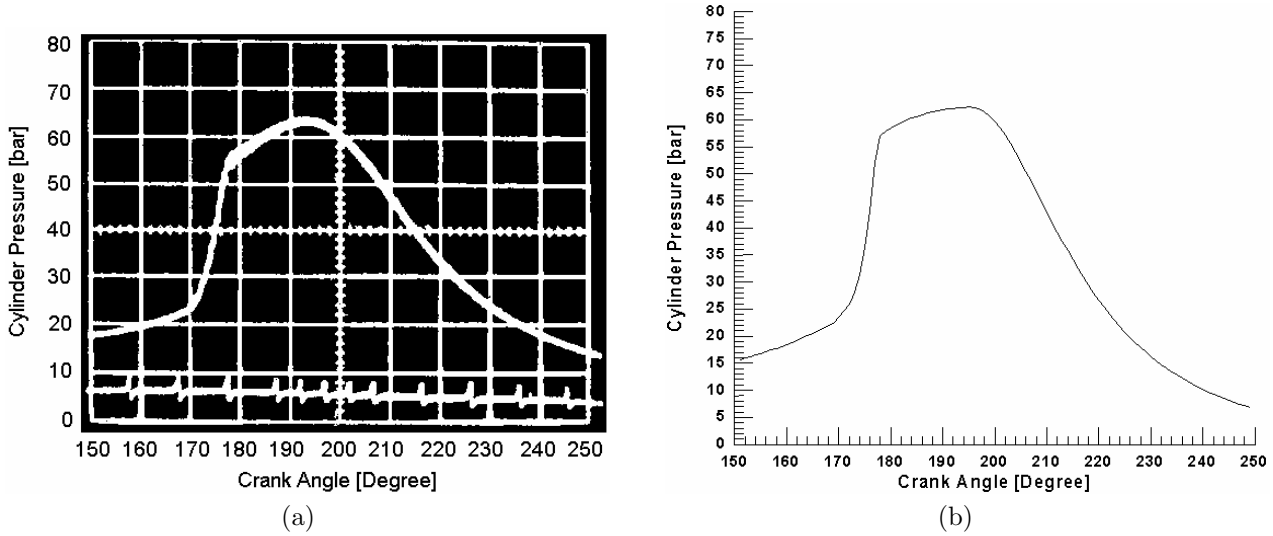

Figure 6. (a) Cylinder pressure with crank angles photograph and (b) model prediction indicating pre-ignition combustion (compression ratio = 10, equivalence ratio = 0.96, engine speed = 25 rev/s, Tin = 313 K, Pin = 1 bar, spark timing = 3° BTDC).

peak temperature and pressure in addition to the reduction in the time required dissociating NO to N_2 and O_2. NOx concentrations decrease as the percentage of alcohol addition increases. This is probably a result of the higher heat of vaporization of alcohol, which reduces the peak temperature inside the cylinder.

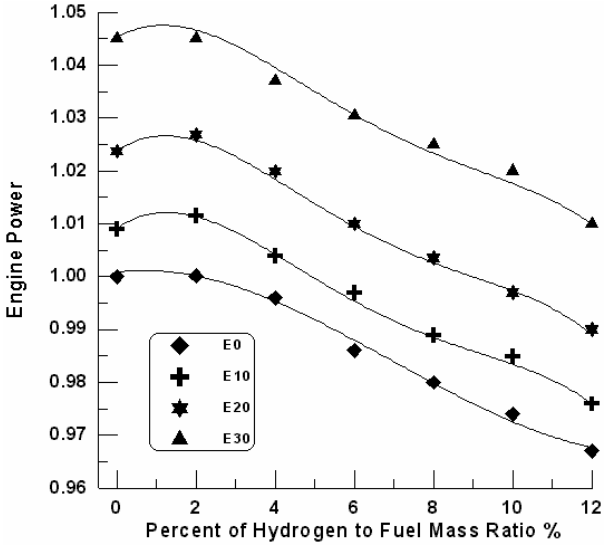

Figure 7. Measurements (symbols) and predictions (solid line) of the effect of hydrogen and/or ethanol blending on the engine power.

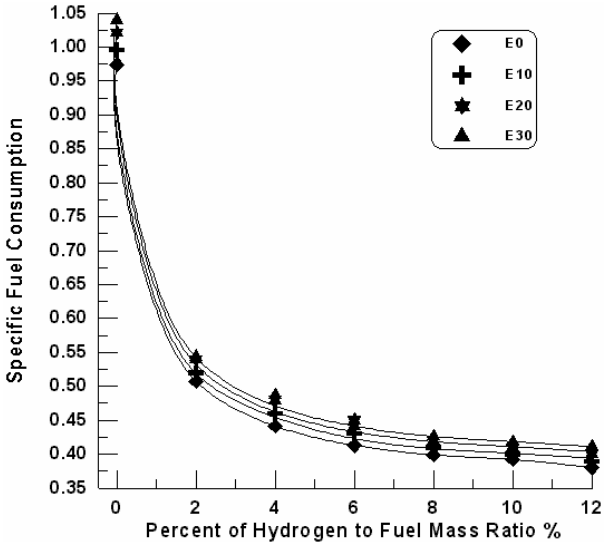

Figure 8. Measurements (symbols) and predictions (solid line) of the effect of hydrogen and/or ethanol blending on the specific fuel consumption.

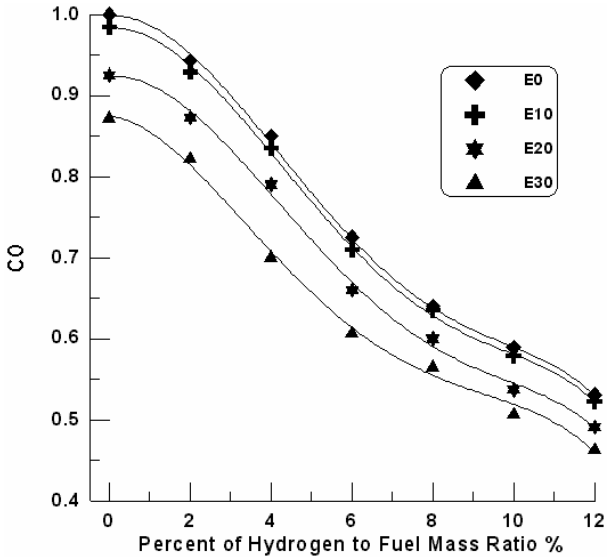

Figure 9. Measurements (symbols) and predictions (solid line) of the effect of hydrogen and/or ethanol blending on the CO emission of the engine.

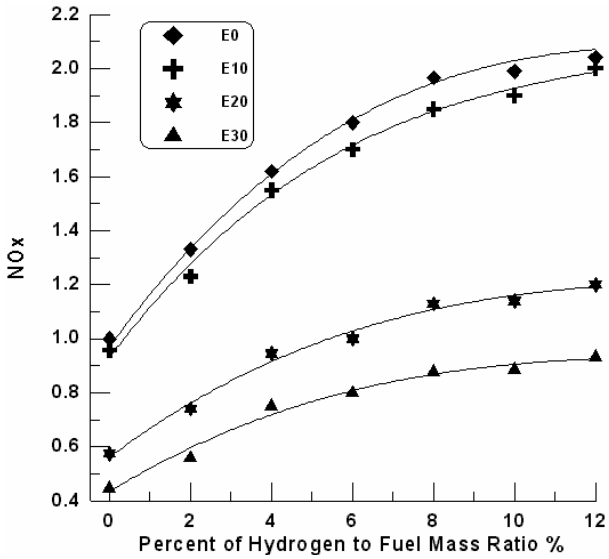

Figure 10. Measurements (symbols) and predictions (solid line) of the effect of hydrogen and/or ethanol blending on the NOx emission of the engine.

Examples of the results of the program computation, of a Ricardo E6/US spark ignition engine operated with a stoichiometric mixture and optimum spark timing for best torque with 7.5 compression ratio and 1500 rpm, are shown in Figures 11-14.

Figure 11 shows the pressure crank angle diagram for 2% mass of hydrogen and 98% mass of liquid fuel (70% gasoline and 30% ethanol by volume), and the corresponding burned and unburned

gas temperature. Figure 12 shows the crank angle diagram of fuel energy, inefficiency effect, crevice flow effect, heat transfer effect and heat release rate. Figure 13 shows the crank angle diagram of flame front speed and flame front radius. The concentration of the combustion product with the crank angle degrees is shown in Figure 14.

Details of the calculation (Figures 11-14) show trends that have been reported by other researchers. This gives confidence in the modeling. The trend of pressure and temperature histories (Figure 11) agrees with a number of published results (Benson et al., 1975; Fagelson et al., 1978; Desoky and El-Emam, 1985; Sher and Hacohen, 1989; North, 1992). The trend of fuel energy, inefficiency effect, crevice flow effect, heat transfer effect, and heat release rate with crank angle (Figure 12) agree with studies by Gatowski et al. (1985), Benson et al. (1975), and Al-Baghdadi and Al-Janabi (2000). The increase in flame radius with angle and the variation in flame speed with angle (Figure 13) agree with test results reported by Benson et al. (1975) and with the work by Al-Baghdadi and Al-Janabi (1999). The prediction of maximum NO and its relationship with the time for freezing (Figure 14) agree well with the works by Fagelson et al. (1978), Benson et al. (1975), and Sher and Hacohen (1989).

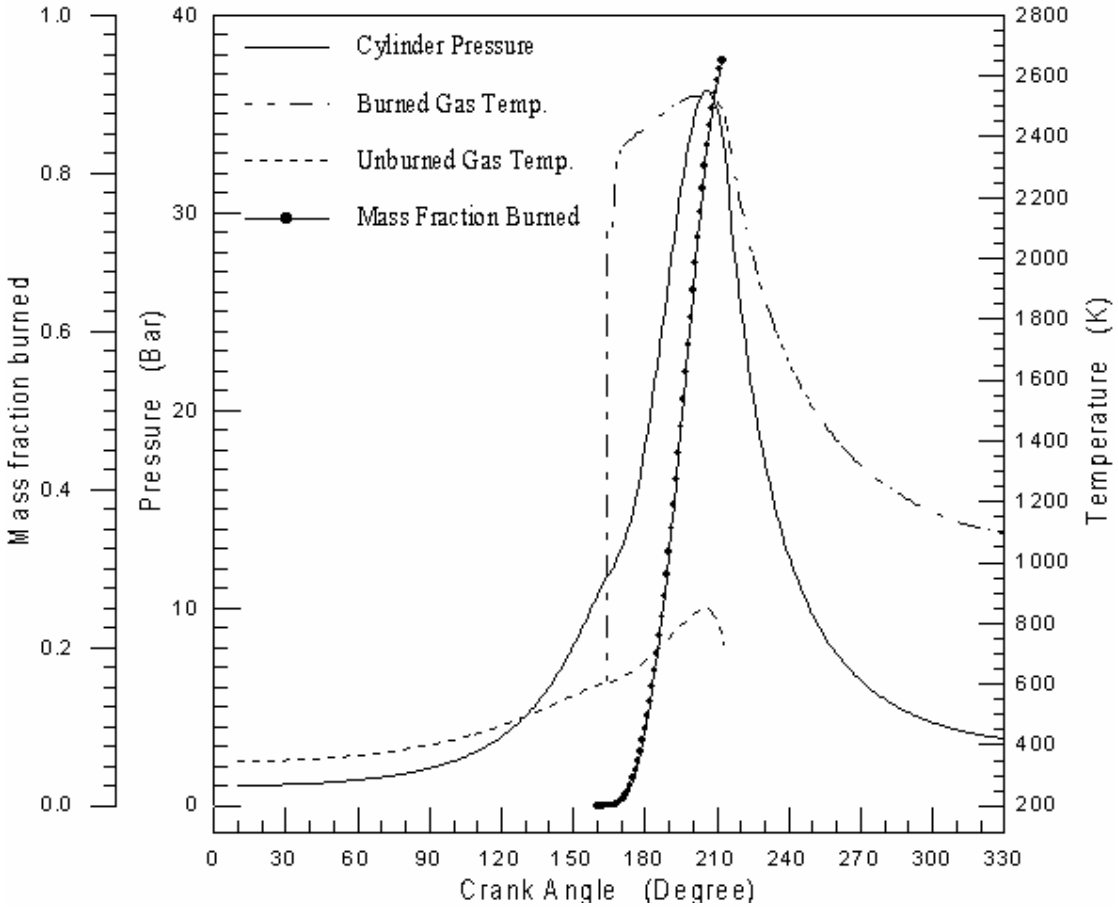

Figure 11. Variation in cylinder pressure, unburned and burned temperature with crank angle.

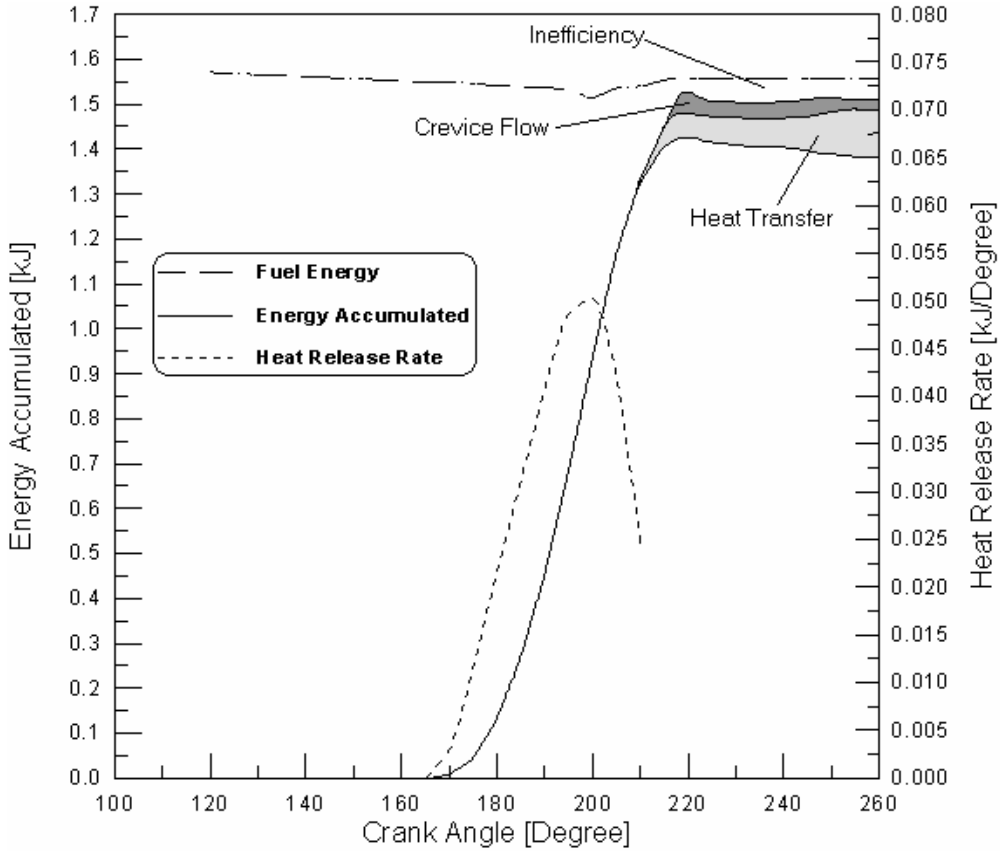

Figure 12. Heat release analysis showing the effects of heat transfer, crevices, and combustion inefficiency.

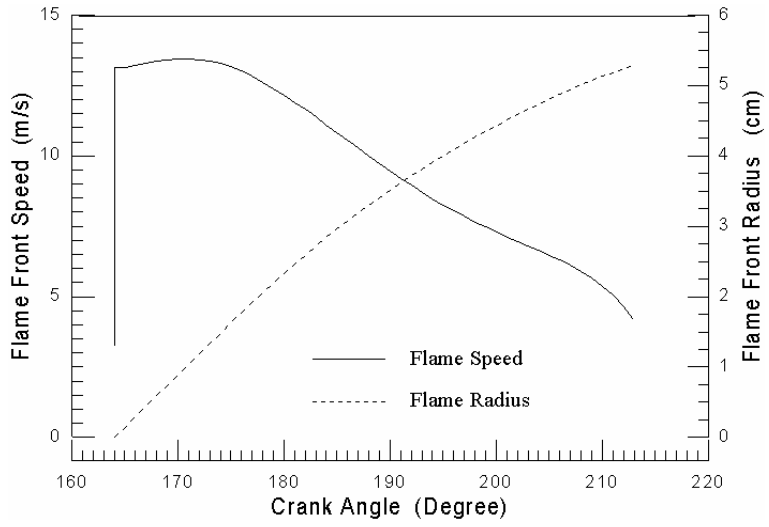

Figure 13. Variation in flame front speed and flame front radius with crank angle.

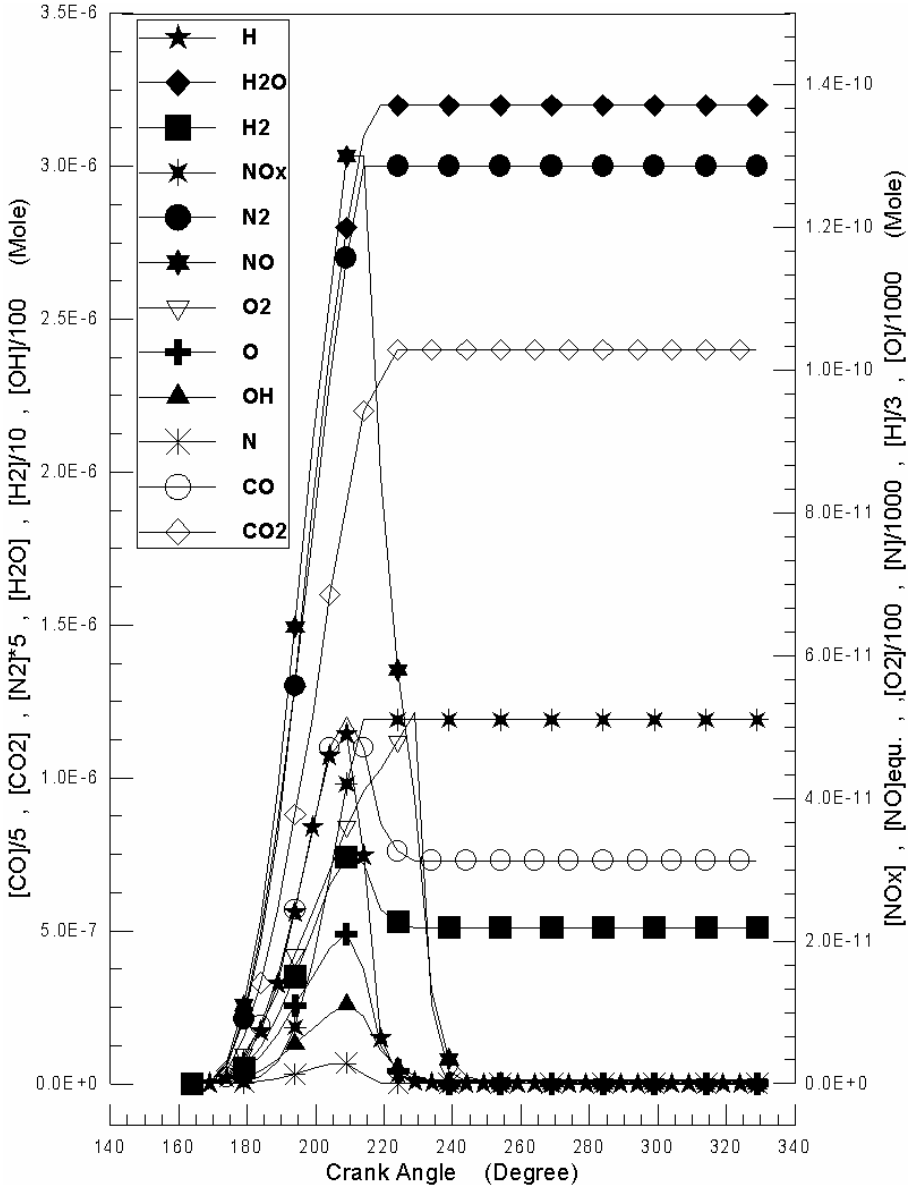

Figure 14. Variation in concentration of combustion products with crank angle.

Conclusion

A mathematical and simulation model has been developed to simulate a 4-stroke cycle of a spark ignition engine fueled with hydrocarbon, hydrogen and ethanol singly or in a blend. The program written from this simulation model can be used to assist in the design of a spark ignition engine for alternative fuels as well as to study many problems such as pre-ignition, knock, pollutant emissions, catalytic devices, exhaust gas re-circulating valves, effects of misfire and maldistribution of the fuel-air mixture. Many other parameters can be studied using this simulation model, such as the effect of combustion duration for each fuel on the performance and emission of the engine, the optimal amount of fuel supplement, and high useful compression ratio for each fuel.

The main results obtained from the present study are as follows:

1. Hydrogen can be used as a supplementary fuel in modern spark ignition engines without major changes, and it can help save a considerable part of the available oil and save our environ-

ment from toxic pollutants.

2. Ethanol can be used as a supplementary fuel up to 30% of gasoline in modern spark ignition engines without major changes, and it improves the output power and reduces the NOx emissions of a hydrogen supplemented fuel engine.

3. The hydrogen added improves the combustion process, especially in the later combustion period, reduces the ignition delay, speeds up the flame front propagation, reduces the combustion duration, and retards the spark timing.

4. The blending of ethanol reduces the CO and NOx emissions and peak temperature.

5. The concentration of CO is reduced, and the concentration of NOx is increased due to hydrogen blending.

6. The engine power is increased until a hydrogen-fuel mass ratio of 2% and ethanol-fuel ratio of 30%.

7. The blending of ethanol or hydrogen increases the heat release rate.

8. The exhaust temperature is reduced, as is the crevices flow energy due to the blending of hydrogen or ethanol fuel.

9. The blending of hydrogen reduces the specific fuel consumption, while ethanol blending increases the specific fuel consumption.

10. The addition of ethanol to gasoline fuel initially increases the Reid vapor pressure of the blended fuels to a maximum at 10% ethanol addition, and then decreases, indicating an increase in evaporative emissions for ethanol-gasoline blended fuels.

11. The addition of ethanol to gasoline fuel enhances the octane number of the blended fuels. An addition of 15% by volume of ethanol to gasoline produces the same effect as the addition of 0.6 g/l of lead or 15% by volume MTBE.

12. The auto-ignition-free operational region tends to narrow significantly with increasing hydrogen-fuel mass ratio, compression ratio, intake pressure and/or intake temperature, and the retarding possibility in spark timing in the operational region was within about 2° to 3° crank angle from the optimum spark timing at near the stoichiometric equivalence ratio. This represents a practical limitation to the improvement of the power and efficiency of hydrogen engines. The auto-ignition-free operational region tends to widen with the addition of ethanol fuel due to a reduction in the peak temperature through the power cycle.

Nomenclature

A	area (m^2)
ae	moles of fuel corresponding to one mole of productions ($kmole$)
B	cylinder bore (m)
C_p	specific heat at constant pressure ($kJ/kmole.K$)
C_v	specific heat at constant volume ($kJ/kmole.K$)
DP	delay period (degree)
e	specific internal energy ($kJ/kmole$)
E	hydrogen activation energy = 83740 $J.mole/K$
f	turbulent flame factor (-)
J	mole ratio of hydrogen fuel addition (-)
k	thermal conductivity ($W/m.K$)
m	number of atomic hydrogen in hydrocarbon fuel ($atom$)
M	mass of gas mixture (kg)
MW	molecular weight of gas mixture ($kg/kmole$)
n	number of atomic carbon in hydrocarbon fuel ($atom$)
N	number of mole ($kmole$)
P	pressure (bar)
Q	energy (kJ)
R	universal gas constant = 8.314 $J.mole/K$
rpm	engine speed (rpm)
S	stroke (m)
SL	laminar flame front speed (m/s)
ST	turbulent flame front speed (m/s)
t	Time (sec)
T	temperature (K)
UP	mean piston speed (m/s)
V	cylinder volume (m^3)
X	mole fraction (-)
Xf	mole fraction of fresh mixture (-)
Xm	mass fraction (-)
Xr	mole fraction of residual gas (-)
$X_{ethanol}$	ethanol volume ratio (-)
$X_{hydrogen}$	hydrogen mass ratio (-)
YH_2	amount of hydrogen addition
Z	mole ratio of ethanol fuel addition (-)

Subscript

Act.	actual
b	burned zone
cr	crevices
fl	flame front
ht	heat transfer
o	reference condition
st.	stoichiometric
u	unburned zone
w	cylinder wall

Greek symbols

μ	kinematic gas viscosity ($kg/m.K$)
ϕ	equivalence ratio (-)
ρ	density of gas mixture (kg/m^3)
σ	Stefan-Boltzman constant = 5.67e-8 (W/m^2K^4)
θ	crank angle (degree)

References

Al-Baghdadi, M.A.R.S and Al-Janabi, H.A.K.S., "A Prediction Study of the Effect of Hydrogen Blending on the Performance and Pollutants Emission of a Four Stroke Spark Ignition Engine", Int. J. Hydrogen Energy, 24, 363-375, 1999.

Al-Baghdadi, M.A.R.S and Al-Janabi, H.A.K.S., "Improvement of Performance and Reduction of Pollutant Emission of a Four Stroke Spark Ignition Engine Fueled with Hydrogen-Gasoline Fuel Mixture", Energy Conversion & Management, 41, 77-91, 2000.

Al-Baghdadi, M.A.R.S., "A Study on the Hydrogen-Ethyl Alcohol Dual Fuel Spark Ignition Engine", Energy Conversion & Management, 43, 199-204, 2002.

Al-Baghdadi, M.A.R.S., "Performance Study of a Four-Stroke Spark Ignition Engine Working With Both of Hydrogen an Ethyl Alcohol as Supplementary Fuel", Int. J. Hydrogen Energy 25, 1005-1009, 2000.

Al-Baghdadi, M.A.R.S., "The Safe Operation Zone of the Spark Ignition Engine Working with Dual Renewable Supplemented Fuels (Hydrogen + Ethyl Alcohol)", Renewable Energy Journal, 22, 579-583, 2001.

Al-Hasan, M., "Effect of Ethanol-Unleaded Gasoline Blends on Engine Performance and Exhaust Emission", Energy Conversion and Management, 44, 1547-1561, 2003.

Annand, W.J.D., "Geometry of Spherical Flame Propagation in a Disc-Shaped Combustion Chamber", Journal of Mechanical Engineering Science, 12, 146-149, 1970.

Bang-Quan, H., Jian-Xin, W., Ji-Ming, H., Xiao-Guang, Y. and Jian-Hua, X., "A Study on Emission Characteristics of an EFI Engine with Ethanol Blended Gasoline Fuels", Atmospheric Environment, 37, 949-957, 2003.

Benson, R.S., Annand, W.J.D. and Baruah, P.C., "A Simulation Model Including Intake and Exhaust Systems for a Single Cylinder Four-Stroke Cycle Spark Ignition Engine", Int. J. Mech. Sci., 17, 97-124, 1975.

Desoky, A.A. and El-Emam, S.H., "A Study on the Combustion of Alternative Fuel in Spark Ignition Engines", Int. J Hydrogen Energy 10, 497-504, 1985.

Douaud, A.M. and Eyzat, P., "Four-Octane-Number Method for Predicting the Anti-Knock Behavior of Fuels and Engines", SAE, paper no.780080, 294-308, 1978.

Fagelson, J.J., McLean, W.J. and De Boer, P.C.T., "Performance and NOx Emissions of Spark Ignited Combustion Engines Using Alternative Fuels Quasi one Dimensional Modeling", Journal of Combustion Science and Technology 18, 47-57, 1978.

Gatowski, J.A., Balles, E.N., Nelson, F.E., Ekchian, J.A. and Heywood, J.B., "Heat Release Analysis of Engine Pressure Data", S.A.E. paper no.841359, 5.961-5.977, 1985.

Heywood, J.B., Internal Combustion Engine Fundamentals. McGraw-Hill, 1989.

Morris, W., Shu, C. and Kim, D., "Bioconversion of Waste Paper to Ethanol", Process Biochemistry, 27, 239-245, 1992.

North, D.C., "Investigation of Hydrogen as an Internal Combustion Fuel", Int. J. Hydrogen Energy, 17, 509-512, 1992.

Sher, E. and Hacohen, Y., "Measurements and Predictions of the Fuel Consumption and Emission of a Spark Ignition Engine Fueled with Hydrogen-Enriched Gasoline", Proc. Instan. Mech. Engrs., 203, 155-162, 1989.

Sher, E. and Hacohen, Y., "On the Modeling of a SI 4-Stroke Cycle Engine Fueled with Hydrogen-Enriched Gasoline", Int. J. Hydrogen Energy, 12, 773-781, 1987.

Veziroglu, T.N. and Barbir, F., "Solar-Hydrogen Energy System: The Choice of the Future", Environmental Conservation, 18, 304-312, 1991.

Veziroglu, T.N., Gurkan, I. and Padki, M.M., "Remediation of Greenhouse Problem Through Replacement of Fossil Fuels by Hydrogen", Int. J. Hydrogen Energy, 14, 257-266, 1989.

Wei-Dong, H., Rong-Hong, C., Tsung-Lin, W. and Ta-Hui, L., "Engine Performance and Pollutant Emission of an SI Engine Using Ethanol-Gasoline Blended Fuels", Atmospheric Environment, 36, 403-410, 2002.

Yu, G., Law, C.K. and Wu, C.K., "Laminar Flame Speeds of Hydrocarbon + Air with Hydrogen Addition", Combustion and Flame, 63, 339-347, 1986.